

Grazing incidence x-ray diffraction studies of lipid-peptide mixed monolayers during shear flow

Pradip Kumar Bera,[†] Ajoy Kumar Kandar,^{†,§} Rema Krishnaswamy,^{†,||}
 Marianne Imp rator-Clerc,[‡] Brigitte Pansu,[‡] Doru Constantin,[‡] Santanu Maiti,[¶]
 Milan K. Sanyal,[¶] and A.K. Sood^{*,†}

[†]*Department of Physics, Indian Institute of Science, Bangalore 560012, India*

[‡]*Laboratoire de Physique des Solides, Unit  Mixte de Recherche 8502 Centre National de la Recherche Scientifique, Universit  Paris-Sud 11, 91405 Orsay Cedex, France*

[¶]*Saha Institute of Nuclear Physics, 1/AF, Bidhannagar, Kolkata-700064, India*

[§]*Soft Condensed Matter, Debye Institute for Nanomaterials Science, Utrecht University, Princetonplein 1, 3584 CC Utrecht, The Netherlands*

^{||}*School of Liberal Studies, Azim Premji University, Bangalore, 560100, India*

E-mail: asood@iisc.ac.in

Abstract

Grazing Incidence X-ray Diffraction (GIXD) studies of monolayers of biomolecules at the air-water interface give quantitative information of in-plane packing, coherence lengths of the ordered (diffracting) domains and orientation of hydrocarbon chains of the model membranes. Rheo-GIXD measurements reveal quantitative changes in the monolayer under shear. Here we report GIXD studies of monolayers of Alamethicin peptide, DPPC lipid and their mixtures at the air-water interface under the application of steady shear stresses. The Alamethicin monolayer and the mixed monolayer show flow jamming transition. On the other hand, pure DPPC monolayer under the constant stress flows steadily with a notable enhancement of

area/molecule, coherence length, and the tilt angle with increasing stress, suggesting fusion of domains during flow. The DPPC-Alamethicin mixed monolayer shows no significant change in the area/DPPC molecule or in the DPPC chain tilt angle but the coherence length of both phases (DPPC and Alamethicin) increases suggesting that the domains of individual phases are merging to bigger size promoting more separation of phases in the system during flow. Our results show that Rheo-GIXD has the potential to explore in-situ molecular structural changes under rheological conditions for a diverse range of confined biomolecules at the interfaces.

Introduction

Langmuir monolayer, a molecularly thin film of amphiphilic molecules stabilized on a liquid-air interface, is an important model system for studying self-organized biological structures such as cell membranes, lung alveoli, etc and also has important industrial applications like in foam, emulsion, etc.¹⁻³ A combination of Grazing Incidence X-ray Diffraction (GIXD), specular x-ray reflectivity (XR) and more recently electrochemical scanning tunneling microscopy (EC-STM) of Langmuir-Blodgett (LB) monolayers have been used to understand different kinds of phase transitions, molecular structure and orientation within domains, formation of single layer and bilayers.⁴⁻⁸ Mixed systems like lipid-cholesterol and lipid-peptide monolayers have been studied to probe the interactions of lipids with other molecules and their relative orientation.⁹⁻¹⁴

Alamethicin is an antimicrobial peptide, produced by many living organisms to defend against gram-negative and gram-positive bacteria, fungi, enveloped viruses, eukaryotic parasites, and even tumor cells. Alamethicin isolated from *Trichoderma viride* has 20 residue peptides with predominantly α -helical structure. In the helical conformation, the length of the molecule is 33 Å. The helix oriented parallel to the interface is called the surface (S) state. If it is inserted into the lipid matrix with the helical axis perpendicular to the interface, it is called the inserted (I) state. The aggregation properties and flow behavior of Alamethicin in the form of Langmuir monolayer were studied using fluorescence microscopy and surface rheology.¹⁵ Fluorescence microscopy showed the coexistence of liquid-expanded and solid phases with the area fraction of solid domains increas-

ing with concentration. Interfacial rheology showed that the peptide monolayer at concentration $800 \text{ \AA}^2/\text{molecule}$ and above has yield stress which increases with surface concentration.

Biological lipid rafts are dynamic self-organized membrane microdomains which can recruit specific peptides and lipids selectively while excluding others.¹⁶ The lipid DPPC shows a variety of different ordered states due to the steric and van der Waals interactions between neighboring head groups and alkyl chains. DPPC monolayers exhibit a disordered liquid-expanded (LE) phase that transforms into a liquid-condensed (LC) phase with long-range orientational and short-range positional order at high concentration. The DPPC monolayer has been studied using in-situ fluorescence microscopy to correlate domain dynamics with shear flow.¹⁷⁻²⁰ In the high concentration limit, the thin domain boundaries were only visible by fluorescence and it was proposed that the interlocked domains give rise to the yield stress response of the LC-DPPC monolayer. The domain topology was preserved for small shear rates. The lipid interaction with peptides and their structural organization are governed by electrostatic and hydrophobic interactions. Recently molecular imaging techniques like STM, surface-enhanced infrared absorption (SEIRA) spectroscopy, etc have revealed hexameric pore formation in the lipid membranes.^{21,22} So far there is no structural study of the model membranes at air-water interface under shear, though in-situ GIXD has been proposed as a potential probe to monitor the dynamic properties of the model membranes.^{3,19}

In this work, we present in-situ interfacial rheology along with GIXD to understand changes in the membrane structure under the non-equilibrium steady state flow condition. Rheo-GIXD measurements are done on the three model systems: Alamethicin, DPPC, and DPPC-Alamethicin mixed monolayers, at different applied stress.

Experimental Details

Materials

The lipid with two hydrocarbon chains *1,2-dipalmitoyl-sn-glycero-3-phosphocholine* (DPPC) and the peptide Alamethicin (all from M/s Avanti Polar Lipids, Inc.) were used without further

purification. A mixture of chloroform and methanol (1:1 v/v) was used as a volatile solvent to dissolve the peptide and lipid molecules. The required amount of the solution was spread on the air-water interface using a microsyringe (M/s Hamilton, 50 μ L) to obtain the interfacial layer between the bi-cone and the co-centric homemade shear cell after the evaporation of the solvent.¹⁵ A deionized water sub-phase (M/s Millipore, with a resistivity of 18.2 M Ω .cm) was used for the DPPC monolayer. For pure Alamethicin and DPPC-Alamethicin (molar ratio [Alamethicin]/[DPPC] = 1:2) mixed monolayers, the sub-phase was the aqueous solution of 0.1 mole NaCl (pH 7), which was adjusted with 10^{-3} mole phosphate buffer (Na₂HPO₄:NaH₂PO₄ 1:1, M/s Merck).

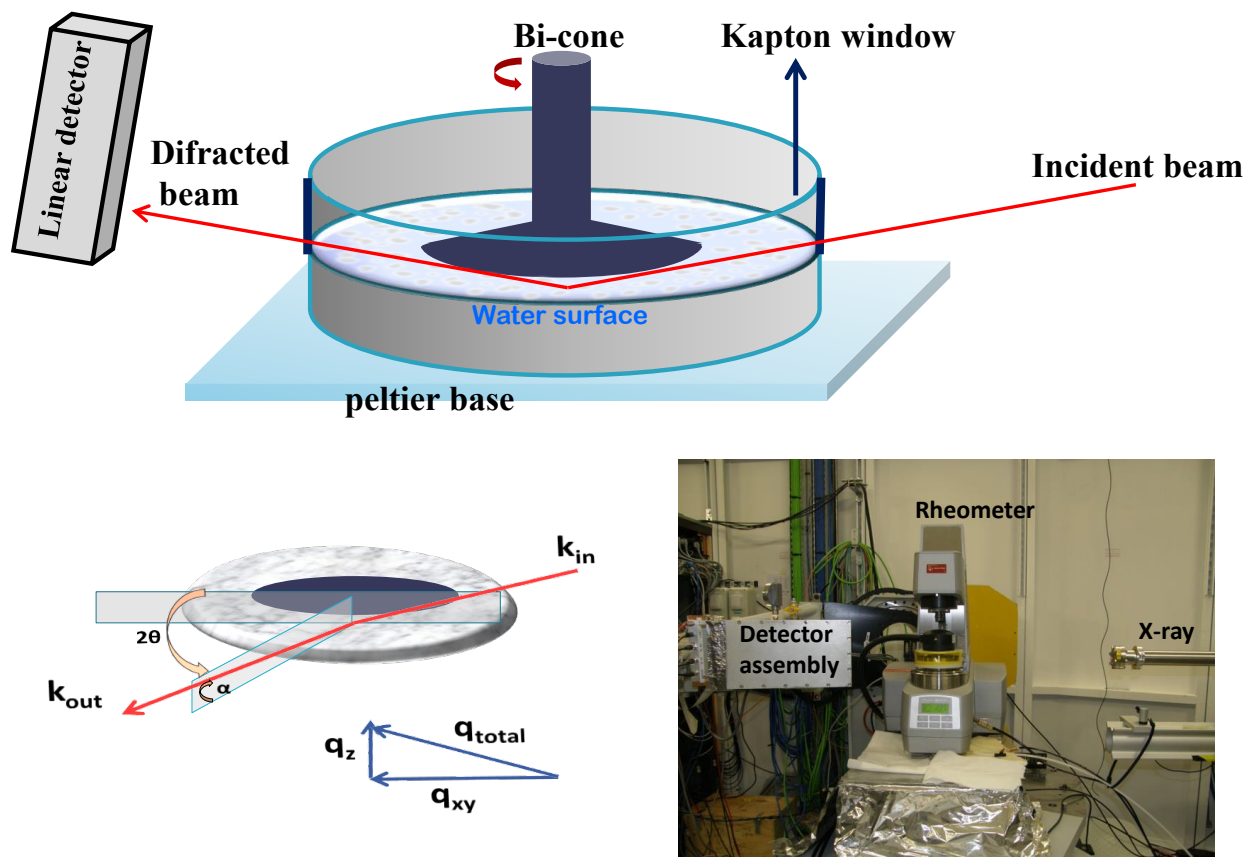


Figure 1: (Color online) Schematic of the in-situ Rheo-GIXD setup, showing the water-filled IRS cell on the rheometer's peltier base, the position of the bi-cone on the interface and the path of the x-ray beam through the Kapton window striking the annular shaped interface (top). Schematic of the GIXD mechanism: in-plane wavevector $q_{xy} = (4\pi/\lambda)\sin(\theta)$ and out-of-plane wavevector $q_z = (2\pi/\lambda)(\sin(\alpha) + \sin(\alpha_i))$ are shown (Bottom left). Photograph of the experimental setup showing the x-ray source, the rheometer on a z-stage and the detector assembly attached to the goniometer (Bottom right).

Rheo-GIXD measurement

After spreading the solution at 300 K the cell was covered by Teflon cover and then waited for 2000 s to let the spreading solvent evaporate under the slow helium flow. During this, an oscillatory shear of strain amplitude $\gamma_0 = 0.001$ with an angular frequency $\omega = 10$ rad/s was applied to follow up the formation of the monolayer. To maintain identical initial conditions before each creep measurement, monolayers were presheared at shear stress $\sigma = 100$ μ Pa for 200 s and then allowed the system to equilibrate for 300 s. After 500 s from the starting of creep measurements, GIXD measurements were started to scan the system in the steady flow state. The rheo-GIXD experiments were carried out at the SIRIUS beamline of the SOLEIL Synchrotron, France using an x-ray photon energy of 8 keV ($\lambda \approx 1.55$ \AA) at 285 K.²³ A stress-controlled rheometer (M/s Anton Paar, model MCR-501) fitted with a homemade interfacial shear cell (radius = 65 mm) based on the bi-cone geometry (radius = 34.14 mm) was mounted on the SIRIUS beamline. A schematic of the experimental setup is shown in Figure 1. The dimension of the x-ray beam footprint on the liquid surface was maintained to be ~ 1.5 mm \times 43 mm (velocity-gradient velocity direction) by the slits attached to the x-ray source. As the x-ray grazing angle is very small, the shear cell was slightly overfilled so that there was an inverted meniscus. The position of the rheometer was set to have the x-ray beam ~ 5 mm away from the cone edge. After each load to place the x-ray beam footprint in the middle of the region, the height of the stage was adjusted with a motor in order to bring the liquid surface to the desired height with the help of laser reflection from the water surface to a fixed camera. Note here the local velocity of the region being scanned is $\approx \dot{\gamma} \times 25$ mm; where $\dot{\gamma}$ is the global shear rate of the system and 25 mm is the distance of the x-ray footprint from the cell wall. Water-saturated helium was injected slowly inside the cell from top to reduce scattering from the air. The monochromatic x-ray beam was adjusted to strike the interface at an incident angle $\alpha_i = 2.28$ mrad, which corresponds to $0.85 \alpha_c$, where α_c is the critical angle of air-water interface¹ for the wavelength used. The linear (1D) gas filled position sensitive detector (PSD) fitted with the goniometer was used to record the diffraction with vertical span $0^\circ \leq \alpha \leq 9^\circ$ and by varying the horizontal angle 2θ from low to high with small steps ($\Delta(2\theta) = 60$ mdeg).

GIXD Data analysis

As a check, a smooth background is observed in GIXD from the clean water surface without any feature. Two dimensional (2D) diffraction plots for all the three monolayers at rest are shown in Figure 2. The in-plane scattering characterized by the wave vector $q_{xy} (= (4\pi/\lambda)\sin(\theta))$ gives information about Bragg peaks in velocity-velocity gradient plane ($V \times \nabla V$) with resolution of 0.005 \AA^{-1} . On the other hand, out-of-plane scattering with $q_z (= (2\pi/\lambda)(\sin(\alpha) + \sin(\alpha_i)))$ gives information about the Bragg rods^{1,13} with resolution of 0.006 \AA^{-1} . In contour plots, peaks are well separated in q_{xy} - q_z plane. We note that the relatively more noise in the data compared to the monolayers prepared in Langmuir trough is expected because our experiment are done on a spread monolayer in place of compressing it from a liquid expanded phase and later, it is in the flow state.^{9,11,13} We have adopted the box integration method for each peak as discussed below. Bragg peaks are observed by integrating the contours from $q_z = 0 \text{ \AA}^{-1}$ to 0.05 \AA^{-1} and from 0.15 \AA^{-1} to 0.25 \AA^{-1} . Bragg peaks are fitted with Voigt function along with background intensity to get the peak centers and the full width at half maximum (FWHM).⁹ For DPPC, lattice distance $d_{hk} = 2\pi/q_{hk}$ are extracted using Bragg peaks q_{02} and q_{11} and then fitted to 2D centered rectangular unit cell model to get the lattice parameters a and b ^{5,13} and hence area/molecule. FWHM of the Bragg peaks were used to determine the coherence length L ($L = 2\pi/\text{FWHM}$).

Bragg rod profiles are obtained by integrating the contours for $\Delta q_{xy} = q_{02} \pm 0.015 \text{ \AA}^{-1}$ (near q_{02}), and $q_{11} \pm 0.030 \text{ \AA}^{-1}$ (near q_{11}) (see Figure 2). In our GIXD data q_{02} and q_{11} peaks have long tails suggesting large variation in the tilt angle of hydrocarbon chains with respect to the interface normal towards the next-nearest-neighbor direction. The maximum tilt angle (δ) is calculated using $\delta = \Delta q_z / (2\pi/a)$, where Δq_z is the maximum peak to peak distance between the Bragg rods.⁹ We have restricted our study for $q_{xy} \geq 1.0 \text{ \AA}^{-1}$, because below this limit, the noise increases significantly towards the direct beam.

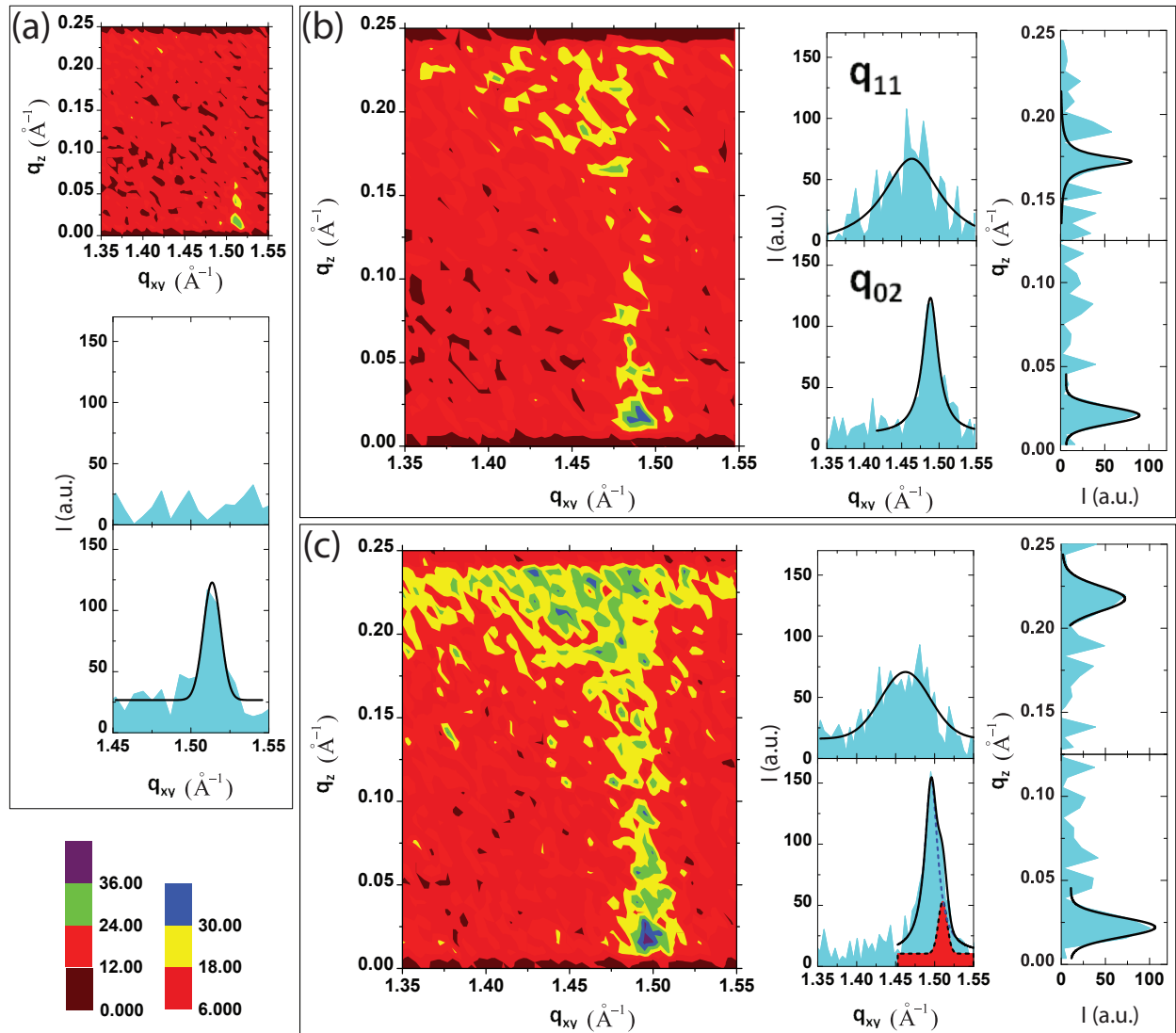


Figure 2: (Color online) GIXD intensity contours in (q_{xy}, q_z) plane, Bragg peaks (I vs q_{xy}) and Bragg rod profiles (I vs q_z) of the three (a) Alamethicin (b) DPPC and (c) DPPC-Alamethicin monolayers are shown under no shear condition at 285 K. Solid lines are fits using Voigt function. In (c) for the bottom Bragg peak, the solid line is the resultant fit with two peaks (blue dotted line and red shaded black dotted line). Color bars represent intensity values in contours.

Results and discussion

Equilibrium study of Alamethicin, DPPC, DPPC-Alamethicin mixed monolayer

Before applying shear to the monolayers at the annular shaped air-water interface between the bi-cone and the shear cell, their structural properties were characterized. Figure 2 shows the equilibrium diffraction patterns of Alamethicin, DPPC, DPPC-Alamethicin mixed monolayer. The Alamethicin monolayer was prepared for $12 \text{ \AA}^2/\text{molecule}$ surface concentration as lower concentrations do not give rise to a measurable diffraction peak in the GIXD. The equilibrium GIXD pattern shows up a strong peak at $q_{xy} = 1.514 \text{ \AA}^{-1}$ near $q_z = 0$ confirming that the Alamethicin molecules are adsorbed on the surface. The observed strong peak due to the Alamethicin corresponds to the pitch of the helix of 4.15 \AA (Figure 3c) which is quite small compared with the pitch of 5.4 \AA for a free α -helix. This reduction in helix pitch is due to the compact packing of Alamethicin molecules on the water surface at this high concentration, consistent with the previous study of the helical scattering distribution of Alamethicin.²⁴ The high coherence length estimated from the measured linewidth ($\sim 475 \text{ \AA}$) suggests that there are domains of at least 14 correlated molecules. The expected hexagonal lattice ordering, forming holes inside these domains,²¹ with lattice parameters of $a = 19 \text{ \AA}$ should show a Bragg peak in the low q range which is not seen in our experiments due to high background intensity near the direct beam, and hence we cannot estimate the area/molecule from the GIXD.

The GIXD pattern from DPPC (solution concentration of 0.5 mg/mL) shown in Figure 2b gives area/molecule = $42.1 \text{ \AA}^2/\text{molecule}$. DPPC has 2D ordering of molecules on the water surface and gives rise to two well-separated two Bragg peaks at $q_{xy} = 1.464 \text{ \AA}^{-1}$ and $q_{xy} = 1.489 \text{ \AA}^{-1}$ (Figure 2b). The relative intensity of these two peaks is $\sim 2:1$ as expected for the DPPC monolayer.⁹ The diffraction pattern is analyzed with the centered-rectangular unit cell model of rod-shaped alkyl chains with uniform molecular tilts towards the nearest neighbors with respect to the layer normal⁹ (Table 1). The coherence length and the hydrocarbon chain tilt angle are consistent with

the previous studies.⁹

The DPPC-Alamethicin mixed monolayer was prepared with molar ratio 1:2 and with surface concentrations $12 \text{ \AA}^2/\text{Alamethicin-molecule}$. The GIXD clearly shows three Bragg peaks (Figure 2c), one is at 1.510 \AA^{-1} representing Alamethicin helix pitch and the other two at 1.463 \AA^{-1} and 1.496 \AA^{-1} with 2:1 intensity ratio, associated with the DPPC molecular ordering in the monolayer. The estimated area/molecule of DPPC is $42.0 \text{ \AA}^2/\text{molecule}$ which is very close to the pure DPPC monolayer (Table 2). The hexagonal structure of the phase separated Alamethicin phase in DPPC-Alamethicin²¹ mixture could not be observed due to the high direct-beam leakage intensity at low q_{xy} . Note that in equilibrium, the Alamethicin helix peak is on the shoulder of the DPPC q_{02} Bragg peak, but with shear flow coherence lengths corresponding to the DPPC q_{02} peak and the Alamethicin helix peak increase drastically and thus Alamethicin helix peak stands well separated in the GIXD pattern (see Figure 5b).

Creep study of the Alamethicin monolayer

We now proceed to examine the structural changes in the monolayers as a function of time under different shear stress condition. Figure 3a shows the creep behavior of Alamethicin monolayer studied as a function of applied stress up to 20 \mu Pa . For all applied stresses (σ), shear rate ($\dot{\gamma}$) increases linearly with time for $\sim 60 \text{ s}$ showing significant shear rejuvenation in the monolayer before going to the final steady state. For $\sigma \leq 8 \text{ \mu Pa}$, after rejuvenation, $\dot{\gamma}$ decays by about two orders of magnitude and at a later time ($t \geq 300 \text{ s}$) it shows large fluctuations with positive and negative values (Figure 3a), a signature of the flow jammed state. In comparison, at 20 \mu Pa , $\dot{\gamma}$ attains a steady state value of $\sim 0.06 \text{ s}^{-1}$. Figure 3b shows the GIXD data at four values of stress, integrated over time from 500 s to 2000 s . The helix peak position remains constant with increasing σ but the line width shows variation reflecting the changes in the domain size (Figure 3c). However, there is no systematic variation of the coherence length with applied stress.

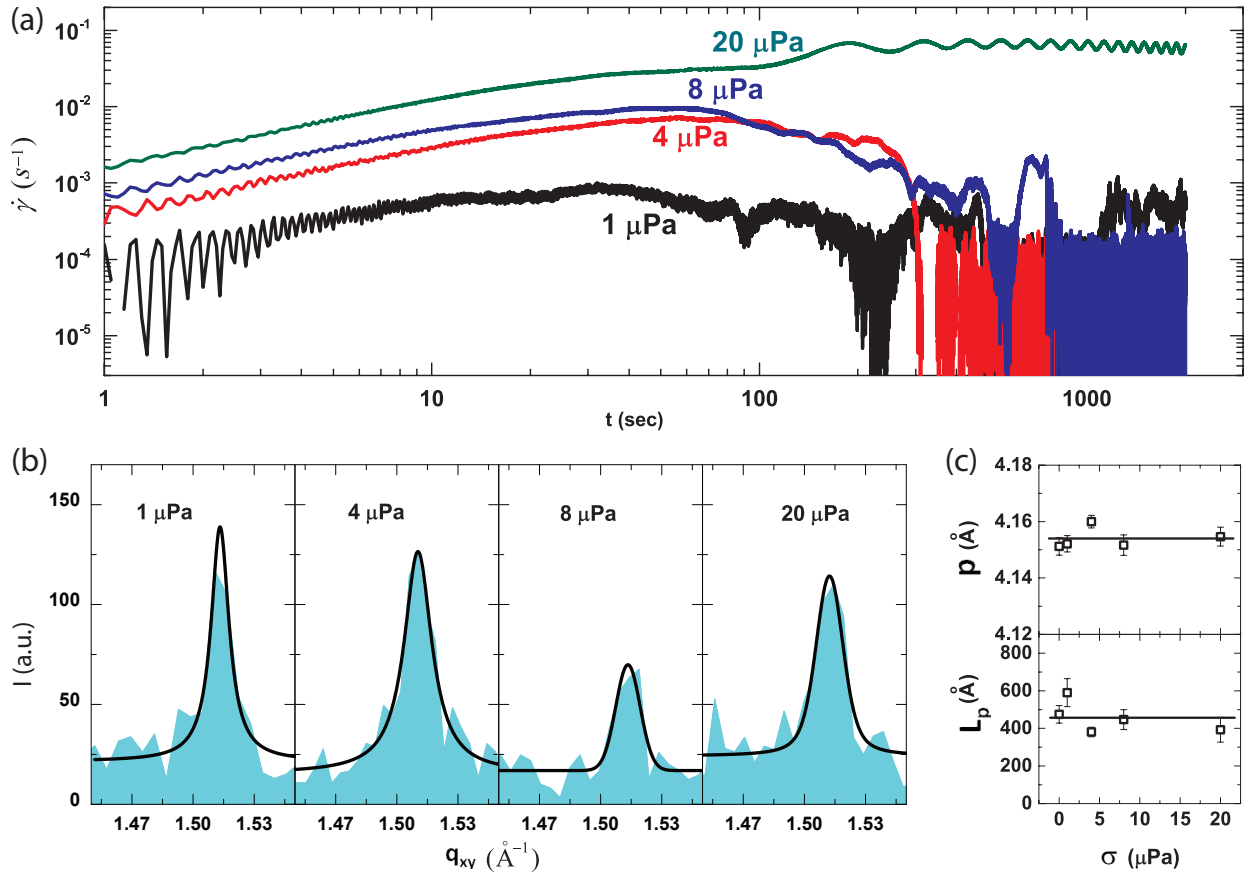


Figure 3: (Color online) Rheo-GIXD creep data of the Alamethicin monolayer (presheared for 200 s followed by 300 s waiting before each measurement; see text): (a) creep curves; shear rate ($\dot{\gamma}$) vs time (t) (applied stress σ is mentioned close to the curves), (b) Bragg peak (I vs q_{xy}) for different σ are shown. Solid lines are fits using Voigt function. The Bragg peak corresponds to the helix pitch of Alamethicin. (c) Helix pitch (p) and coherence length (L_p) are plotted vs σ . Straight horizontal lines represent average values of p and L_p respectively.

Creep study of the DPPC monolayer

The creep behavior of the DPPC monolayer was studied up to 40 μPa (Figure 4). Unlike Alamethicin monolayer, DPPC shows neither substantial shear rejuvenation nor flow jamming. For a given σ , the steady state shear rate is an order of magnitude low compared to Alamethicin monolayer (see 20 μPa data). The Bragg peaks q_{02} , q_{11} , and Bragg rod profiles are shown in Figure 4b-d. The peak position of q_{02} does not change with stress whereas q_{11} peak position shifts to lower values, suggesting elongation of the unit cell under shear flow. Additionally, the width of q_{02} decreases with increasing σ , suggesting fusion of domains during flow. The tilt angle of the hydrocarbon chains increases with σ (Figure 4d). Table-1 summarizes these results and are plotted in Figure 6. The Rheo-GIXD data bring out that the DPPC domains increase in size under applied stress.

Table 1: Structural packing parameters of DPPC monolayer for different σ .

σ [μPa]	d-spacings [\AA]	unit cell dimensions [\AA]	$A_{molecule}$ [\AA^2]	Coherence length [\AA]	Tilt angle δ [$^\circ$]
0	$d_{11} = 4.293 \pm 0.015$ $d_{02} = 4.221 \pm 0.003$	$a = 4.986 \pm 0.024$ $b = 8.443 \pm 0.006$	42.09 ± 0.23	$L_{11} = 76 \pm 7$ $L_{02} = 256 \pm 15$	6.9 ± 0.2
4	$d_{11} = 4.328 \pm 0.010$ $d_{02} = 4.218 \pm 0.002$	$a = 5.042 \pm 0.017$ $b = 8.437 \pm 0.004$	42.54 ± 0.16	$L_{11} = 69 \pm 5$ $L_{02} = 314 \pm 40$	7.9 ± 0.2
8	$d_{11} = 4.350 \pm 0.009$ $d_{02} = 4.229 \pm 0.002$	$a = 5.072 \pm 0.015$ $b = 8.459 \pm 0.005$	42.90 ± 0.15	$L_{11} = 83 \pm 6$ $L_{02} = 627 \pm 103$	9.6 ± 0.3
20	$d_{11} = 4.384 \pm 0.012$ $d_{02} = 4.236 \pm 0.002$	$a = 5.123 \pm 0.020$ $b = 8.472 \pm 0.004$	43.40 ± 0.19	$L_{11} = 74 \pm 6$ $L_{02} = 620 \pm 55$	9.9 ± 0.5
40	$d_{11} = 4.359 \pm 0.005$ $d_{02} = 4.227 \pm 0.002$	$a = 5.088 \pm 0.008$ $b = 8.455 \pm 0.003$	43.02 ± 0.08	$L_{11} = 106 \pm 5$ $L_{02} = 447 \pm 29$	9.8 ± 0.4

Creep study of the mixed monolayer

Figure 5 shows the creep behavior of the DPPC-Alamethicin mixed monolayer studied up to 60 μPa . Shear rejuvenation is observed with $\dot{\gamma}$ increasing linearly with time. At 10 μPa it shows rejuvenation up to 30 s and then goes to the flow jammed state after 60 s of flow similar to the pure Alamethicin monolayer. At 20 μPa and above it goes to a steady flow state with an enhanced

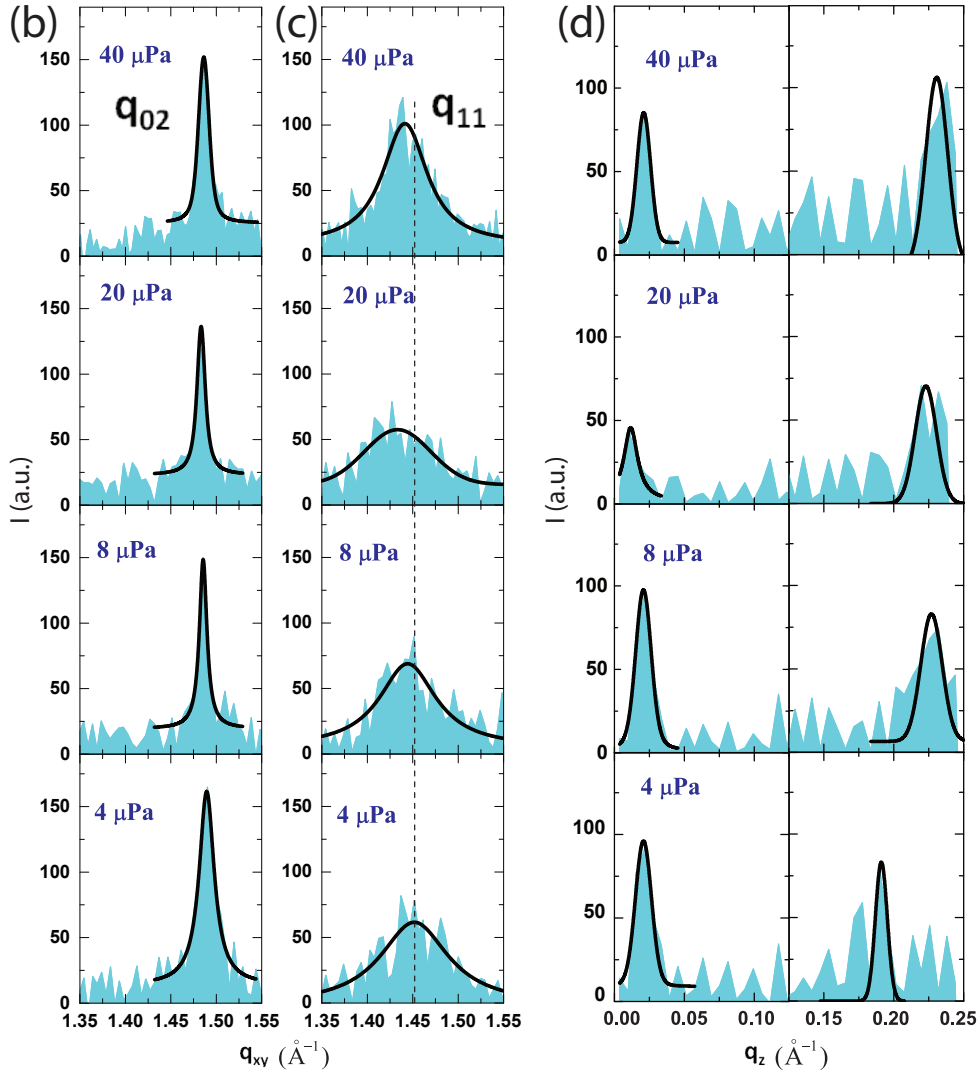
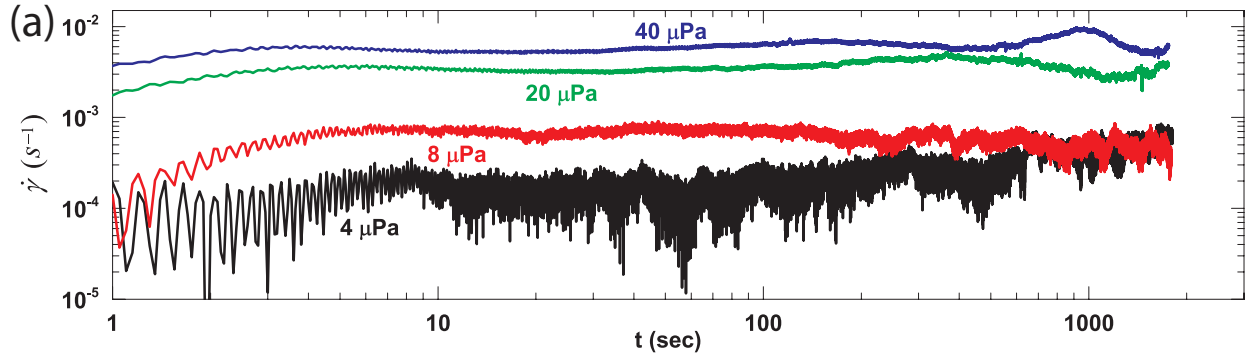


Figure 4: (Color online) Rheo-GIXD creep data of the DPPC monolayer (presheared for 200 s followed by 300 s waiting before each measurement; see text): (a) creep curves; $\dot{\gamma}$ vs t , (b) Bragg peak q_{02} , (c) Bragg peak q_{11} , (d) Bragg rod profile for different σ are shown. Solid lines in (b-d) are fits using Voigt function. Dashed vertical line in (c) has position $q_{xy} = 1.451 \text{ \AA}^{-1}$.

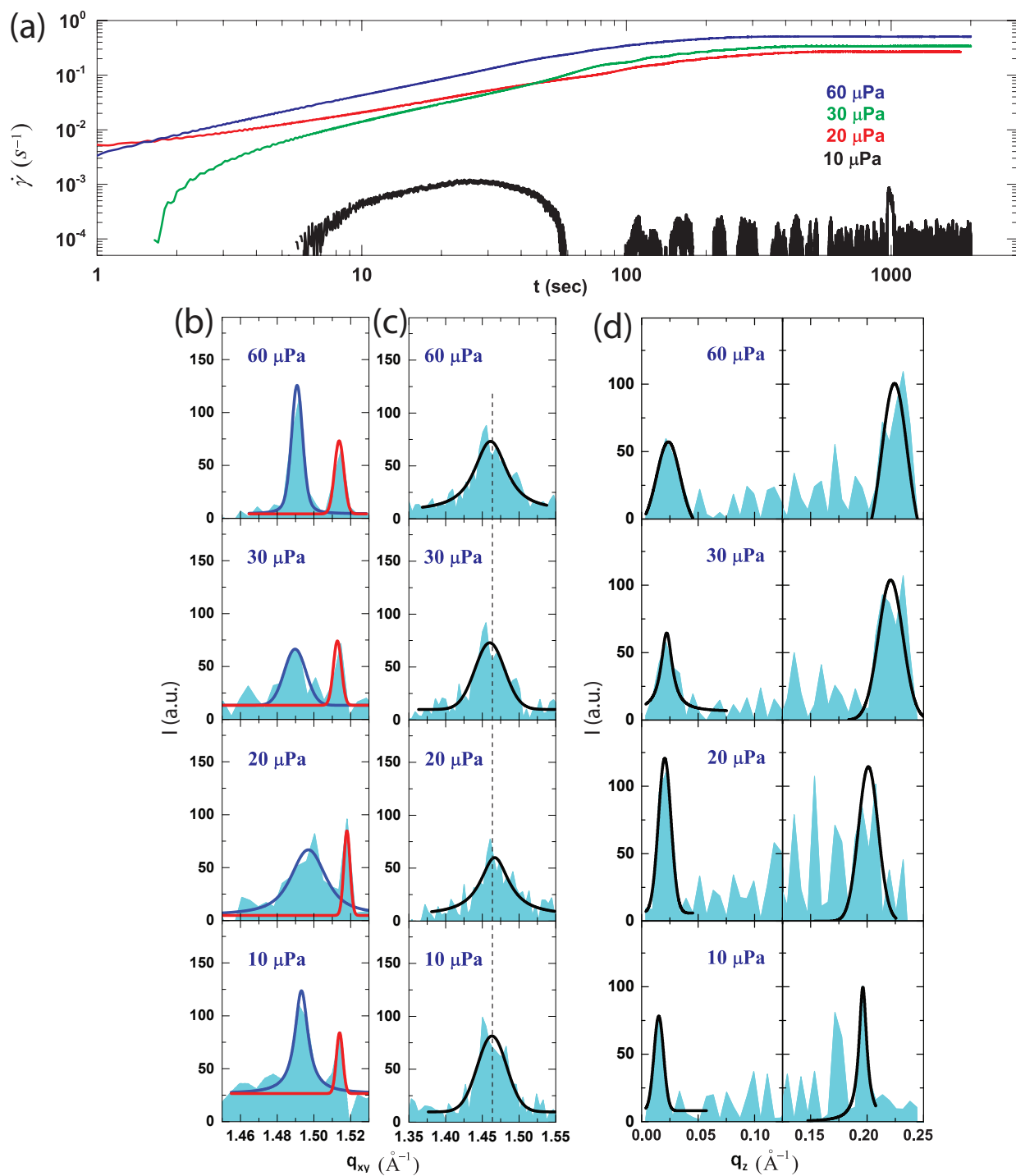


Figure 5: (Color online) Rheo-GIXD creep data of the DPPC-Alamethicin mixed monolayer with molar ratio P/L=1/2 (presheared for 200 s followed by 300 s waiting before each measurement; see text): (a) creep curves; $\dot{\gamma}$ vs t , (b) Bragg peak q_{02} (blue solid fit), Alamethicin helix peak (red solid fit), (c) Bragg peak q_{11} , (d) Bragg rod profile for different σ are shown. Solid lines in (b-d) are fits using Voigt function. Dashed vertical line in (c) has position $q_{xy} = 1.463 \text{ \AA}^{-1}$.

$\dot{\gamma}$ compared to pure Alamethicin monolayer, which is orders of magnitude higher compared to pure DPPC monolayer. This suggests that the DPPC domains are no longer closely packed in the mixed monolayer and stay phase separated with Alamethicin even under high shear rates. Unlike pure DPPC monolayer, peak position of q_{02} and q_{11} do not change under flow (Table 2). Also, the tilt angle remains fixed with increasing σ . Strikingly Alamethicin helix coherence length increases with σ suggesting that the Alamethicin domains are merging to bigger size promoting more separation of phases in the system.

Table 2: Structural packing parameters of DPPC-Alamethicin mixed monolayer for different σ .

σ [μPa]	DPPC d-spacings, Alamethicin pitch [\AA]	DPPC unit cell dimensions [\AA]	DPPC $A_{molecule}$ [\AA^2]	Coherence length [\AA]; DPPC L_{hk} , Alamethicin L_p	Tilt angle δ [$^\circ$]
0	$d_{11} = 4.296 \pm 0.009$ $d_{02} = 4.201 \pm 0.003$ $p = 4.160 \pm 0.005$	$a = 4.999 \pm 0.016$ $b = 8.402 \pm 0.005$	42.00 ± 0.16	$L_{11} = 85 \pm 6$ $L_{02} = 314 \pm 17$ $L_p = 396 \pm 96$	8.9 ± 0.1
10	$d_{11} = 4.294 \pm 0.005$ $d_{02} = 4.208 \pm 0.003$ $p = 4.150 \pm 0.005$	$a = 4.993 \pm 0.008$ $b = 8.416 \pm 0.007$	42.02 ± 0.10	$L_{11} = 134 \pm 8$ $L_{02} = 741 \pm 92$ $L_p = 1510 \pm 459$	8.3 ± 0.2
20	$d_{11} = 4.284 \pm 0.007$ $d_{02} = 4.197 \pm 0.004$ $p = 4.140 \pm 0.003$	$a = 4.981 \pm 0.012$ $b = 8.395 \pm 0.009$	41.81 ± 0.15	$L_{11} = 134 \pm 11$ $L_{02} = 321 \pm 36$ $L_p = 1611 \pm 305$	8.2 ± 0.2
30	$d_{11} = 4.303 \pm 0.005$ $d_{02} = 4.218 \pm 0.004$ $p = 4.153 \pm 0.006$	$a = 5.003 \pm 0.009$ $b = 8.435 \pm 0.008$	42.20 ± 0.12	$L_{11} = 132 \pm 8$ $L_{02} = 413 \pm 58$ $L_p = 1250 \pm 355$	9.1 ± 0.4
60	$d_{11} = 4.300 \pm 0.005$ $d_{02} = 4.215 \pm 0.001$ $p = 4.151 \pm 0.002$	$a = 4.999 \pm 0.008$ $b = 8.429 \pm 0.001$	42.14 ± 0.07	$L_{11} = 120 \pm 17$ $L_{02} = 772 \pm 31$ $L_p = 1050 \pm 91$	9.2 ± 0.3

For comparison we have plotted area/molecule ($A_{molecule}$), coherence lengths (L_{hk}) and the tilt angle (δ) of DPPC for pure and mixed systems (Figure 6a-d). For pure DPPC monolayer, the area/molecule (Figure 6a) increases rapidly with σ and saturates at high values, whereas for mixed monolayer it does not change with σ . The coherence length in [02] direction has a rapid increment for the pure DPPC monolayer but fluctuates for the mixed monolayer. On the other hand, the coherence length in [11] direction has a slow increment for the pure DPPC monolayer but has a rapid increment for the mixed monolayer. For pure DPPC monolayer, the tilt angle increases and

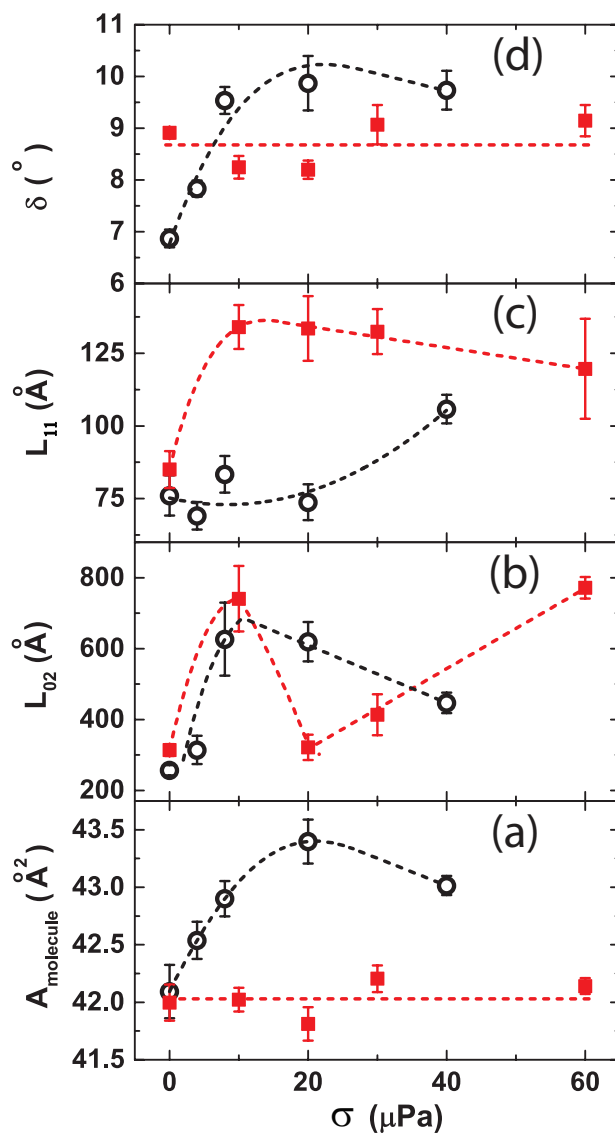


Figure 6: (Color online) Area/molecule of DPPC (A_{molecule}), coherence length corresponding to two DPPC Bragg peaks L_{02} ; L_{11} , tilt angle of DPPC chains (δ) for pure DPPC (open circles) and DPPC-Alamethicin mixed (red squares) monolayers are plotted against σ . Dotted curves are guides to the eyes.

then saturates for higher σ , but in the mixed monolayer, it is $\sim 9^\circ$ for all σ .

Conclusions

We have described the methodology of Rheo-GIXD, an extension of the well established GIXD technique to study molecular structure under steady shear on the interface by combining Interfacial rheology and GIXD. We have demonstrated that the GIXD signal can be captured even when interfacial molecular domains move under shear. At low σ , pure Alamethicin as well as mixed monolayer show jamming behavior after about ~ 100 sec. Rheo-GIXD measurements show that DPPC 2D crystals are stable under shear flow, with significant changes in their lattice parameters and tilt of the hydrophobic chains. The presence of buffer sub-phase stabilizes the peptide at the air-water interface, but does not lead to the binding of the peptide with DPPC head group, as inferred from the observation that, the scattering signal is almost similar in both cases (pure DPPC and DPPC-Alamethicin mixed). The phase separation and the barrel-stave aggregation of an amphipathic peptide in a peptide-lipid matrix in equilibrium²¹ is also consistent with our Rheo-GIXD observations under shear. We have shown that, the peptide 2D crystals grow bigger in size by merging domains under shear. The structural properties of hexameric pores could not be probed here due to high direct-beam leakage in low q_{xy} region.

Further work along with x-ray reflectivity study on this system will allow us to study the dependence of structural parameters on the velocity gradient. Also, this technique can be used to probe the solid-like to fluid-like transition under the oscillatory shear deformation. We believe that our results will provide motivation for studying the molecular level structure of many other membranes in non-equilibrium conditions.

Acknowledgement

A.K.S. thanks Department of Science and Technology (DST), India for the support through Year of Science Professorship. M.K.S. acknowledges the support Raja Ramanna Fellowship of De-

partment of Atomic Energy (DAE). R. K. thanks DST for the Ramanujan Fellowship. A.K.K. and P.K.B. thank University Grants Commission (UGC) for the D.S.Kothari fellowship and Senior Research Fellowship, respectively. We thank DST for financial assistance through CEFIPRA-SOLEIL-Synchrotron Programme (20140232, AP14/15) to use the Synchrotron Beamtime. We acknowledge SOLEIL for provision of synchrotron radiation facilities and we thank P. Fontaine and N. Aubert for assistance in using the beamline SIRIUS. We thank Prof. Jean Daillant for fruitful discussions.

References

- (1) Als-Nielsen, J.; Jacquemain, D.; Kjaer, K.; Leveiller, F.; Lahav, M.; Leiserowitz, L. Principles and applications of grazing incidence x-ray and neutron scattering from ordered molecular monolayers at the air-water interface. *Physics Reports* **1994**, *246*, 251–313.
- (2) Kaganer, V. M.; Möhwald, H.; Dutta, P. Structure and phase transitions in Langmuir monolayers. *Reviews of Modern Physics* **1999**, *71*, 779.
- (3) Fuller, G. G.; Vermant, J. Complex fluid-fluid interfaces: rheology and structure. *Annual Review of Biophysics and Biomolecular Structure* **2012**, *3*, 519–543.
- (4) Kjaer, K.; Als-Nielsen, J.; Helm, C.; Laxhuber, L.; Möhwald, H. Ordering in lipid monolayers studied by synchrotron x-ray diffraction and fluorescence microscopy. *Physical Review Letters* **1987**, *58*, 2224.
- (5) Kjaer, K. Some simple ideas on x-ray reflection and grazing-incidence diffraction from thin surfactant films. *Physica B: Condensed Matter* **1994**, *198*, 100–109.
- (6) Miller, C.; Majewski, J.; Watkins, E.; Mulder, D.; Gog, T.; Kuhl, T. Probing the local order of single phospholipid membranes using grazing incidence x-ray diffraction. *Physical Review Letters* **2008**, *100*, 058103.

- (7) Maiti, S.; Sanyal, M. K.; Mukhopadhyay, M. K.; Singh, A.; Mukherjee, S.; Datta, A.; Fontaine, P. Structural and optical properties of two-dimensional gadolinium stearate Langmuir monolayer. *Chemical Physics Letters* **2018**, *712*, 177–183.
- (8) Maiti, S.; Maiti, S.; Maier, A.; Hagenlocher, J.; Chumakov, A.; Schreiber, F.; Scheele, M. Understanding the Formation of Conductive Mesocrystalline Superlattices with Cubic PbS Nanocrystals at the Liquid/Air Interface. *The Journal of Physical Chemistry C* **2018**, *123*, 1519–1526.
- (9) Watkins, E.; Miller, C.; Mulder, D.; Kuhl, T.; Majewski, J. Structure and orientational texture of self-organizing lipid bilayers. *Physical Review Letters* **2009**, *102*, 238101.
- (10) Wu, G.; Majewski, J.; Ege, C.; Kjaer, K.; Weygand, M. J.; Lee, K. Y. C. Interaction between lipid monolayers and poloxamer 188: an X-ray reflectivity and diffraction study. *Biophysical Journal* **2005**, *89*, 3159–3173.
- (11) Neville, F.; Ishitsuka, Y.; Hodges, C. S.; Konovalov, O.; Waring, A. J.; Lehrer, R.; Lee, K. Y. C.; Gidalevitz, D. Protegrin interaction with lipid monolayers: grazing incidence X-ray diffraction and X-ray reflectivity study. *Soft Matter* **2008**, *4*, 1665–1674.
- (12) Ivankin, A.; Kuzmenko, I.; Gidalevitz, D. Cholesterol-phospholipid interactions: new insights from surface x-ray scattering data. *Physical Review Letters* **2010**, *104*, 108101.
- (13) Watkins, E.; Miller, C.; Majewski, J.; Kuhl, T. Membrane texture induced by specific protein binding and receptor clustering: active roles for lipids in cellular function. *Proceedings of the National Academy of Sciences* **2011**, *108*, 6975–6980.
- (14) Broniatowski, M.; Sobolewska, K.; Flasiński, M.; Wydro, P. Studies on the interactions of bisphenols with anionic phospholipids of decomposer membranes in model systems. *Biochimica et Biophysica Acta (BBA)-Biomembranes* **2016**, *1858*, 756–766.

- (15) Krishnaswamy, R.; Rathee, V.; Sood, A. Aggregation of a Peptide Antibiotic Alamethicin at the Air- Water Interface and Its Influence on the Viscoelasticity of Phospholipid Monolayers. *Langmuir* **2008**, *24*, 11770–11777.
- (16) Edidin, M. The state of lipid rafts: from model membranes to cells. *Annual Review of Biophysics and Biomolecular Structure* **2003**, *32*, 257–283.
- (17) Espinosa, G.; López-Montero, I.; Monroy, F.; Langevin, D. Shear rheology of lipid monolayers and insights on membrane fluidity. *Proceedings of the National Academy of Sciences* **2011**, *108*, 6008–6013.
- (18) Hermans, E.; Vermant, J. Interfacial shear rheology of DPPC under physiologically relevant conditions. *Soft Matter* **2014**, *10*, 175–186.
- (19) Kim, K.; Choi, S. Q.; Zasadzinski, J. A.; Squires, T. M. Interfacial microrheology of DPPC monolayers at the air–water interface. *Soft Matter* **2011**, *7*, 7782–7789.
- (20) Choi, S.; Steltenkamp, S.; Zasadzinski, J.; Squires, T. Active microrheology and simultaneous visualization of sheared phospholipid monolayers. *Nature Communications* **2011**, *2*, 312.
- (21) Pieta, P.; Mirza, J.; Lipkowski, J. Direct visualization of the alamethicin pore formed in a planar phospholipid matrix. *Proceedings of the National Academy of Sciences* **2012**, *109*, 21223–21227.
- (22) Forbrig, E.; Staffa, J. K.; Salewski, J.; Mroginski, M. A.; Hildebrandt, P.; Kozuch, J. Monitoring the orientational changes of Alamethicin during incorporation into bilayer lipid membranes. *Langmuir* **2018**, *34*, 2373–2385.
- (23) Fontaine, P.; Ciatto, G.; Aubert, N.; Goldmann, M. Soft interfaces and resonant investigation on undulator source: a surface X-ray scattering beamline to study organic molecular films at the SOLEIL synchrotron. *Science of advanced materials* **2014**, *6*, 2312–2316.

- (24) Spaar, A.; Münster, C.; Salditt, T. Conformation of peptides in lipid membranes studied by X-ray grazing incidence scattering. *Biophysical Journal* **2004**, *87*, 396–407.